ACS NANO

www.acsnano.org

ARTICLE

Cryo-Shocked Platelet Coupled with ROS-Responsive Nanomedicine for Targeted Treatment of Thromboembolic Disease

Xingping Quan, Xiao Liang, Yuanfu Ding, Yan Han, Junyan Li, Mengchen Yuan, Yiyang Li, Zhen Yuan, Ruibing Wang,* and Yonghua Zhao*

Cite This: *ACS Nano* 2023, 17, 6519−6533

Read Online

ACCESS | Metrics & More | Article Recommendations | Supporting Information

ABSTRACT: **Thrombolysis with tissue plasminogen activator (tPA) provides the most common therapy for ischemic stroke onset within the past 4.5 h. However, enhanced neutrophil infiltration and secondary blood-brain barrier injury caused by tPA administration have limited its therapeutic application, and tPA treatment is often accompanied by hemorrhagic transformation. To overcome the limitations of thrombolysis by tPA, maximize the therapeutic efficacy, and improve the safety, herein, we report a cryo-shocked platelet-based cell-hitchhiking drug delivery system, which consists of cryo-shocked platelet (CsPLT) and reactive oxygen species (ROS)-responsive liposomes loaded with thrombolytic tPA and anti-inflammation drug aspirin (ASA). CsPLT and liposomes were facilely conjugated via host−guest interactions. Under the guidance of CsPLT, it selectively accumulated in the thrombus site and quickly released the therapeutic payloads in response to the high ROS. tPA subsequently exhibited localized thrombolytic activity to suppress the expansion of thrombus, while ASA assisted in the inactivation of reactive astrogliosis, microglial/macrophage, and obstruction of neutrophil infiltration. This cryo-shocked platelet-hitchhiking tPA/ASA delivery system not only improves the thrombus-targeting efficiency of the two drugs for highly localized thrombolytic effects and anti-inflammation actions and platelets inactivation but also provides insights to the development of targeted drug delivery systems for thromboembolic disease treatment.**

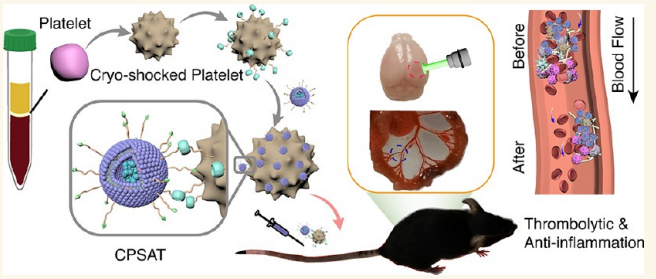

KEYWORDS: *Cryo-shocked platelet, hitchhiking, supramolecular nanomedicine, ROS-responsive, thromboembolic disease*

INTRODUCTION

Thromboembolic disease is an intravascular event with over 25% fatality ratio, which usually occurs during or after the formation of thrombus and vascular obstruction, mainly induced by arterial or venous thrombosis, e.g., ischemic stroke and mesenteric ischemia.[1−5] Ischemic stroke occurs after the cerebral vessel is suddenly narrowed or blocked by thrombus, leading to a shortage or suspension of blood flow,[6] while mesenteric ischemia is another thrombus-related disease complicated with inadequate intestinal blood flow, necrosis, or perforation.[7] For these thrombi-driven diseases, the adhesion and aggregation of platelets, as well as deposition of fibrin, are commonly observed. Hypoxia induced by vascular obstruction promotes the generation of reactive oxygen species (ROS), causing the high permeability of barrier and infiltration of immune cells.[8−10] Targeted delivery of therapeutic agents to the thrombus site based on these individual characteristics may contribute to more satisfactory therapeutic outcomes.

Although antiplatelet agents and anticoagulants are commonly administered for antithrombotic therapy, the side effects (e.g., hemorrhage) of this approach, caused by off-target activities and high dosage, often compromise the therapeutic efficacy. Aspirin (acetylsalicylic acid, ASA), an inhibitor of enzyme cyclooxygenase COX-1/2, can suppress the platelets activation at a low dose by reducing the generation of thromboxane A_2 (TXA_2) and can preferentially inhibit the inflammation reaction by decreasing the release of prostaglandins E_2 (PGE_2).[11,12] In fact, it has been recognized that a low dose of ASA can effectively prevent thromboembolic disease.[13−15] In addition, ASA also inhibits the formation of

Received: November 28, 2022
Accepted: March 21, 2023
Published: March 27, 2023

Scheme 1. Scheme Showing Preparation of Platelet-Derived CPSAT and Delivery of ROS-Responsive Nanoparticles to Thrombus with Enhanced Thrombolytic and Anti-Inflammatory Efficacies[a]

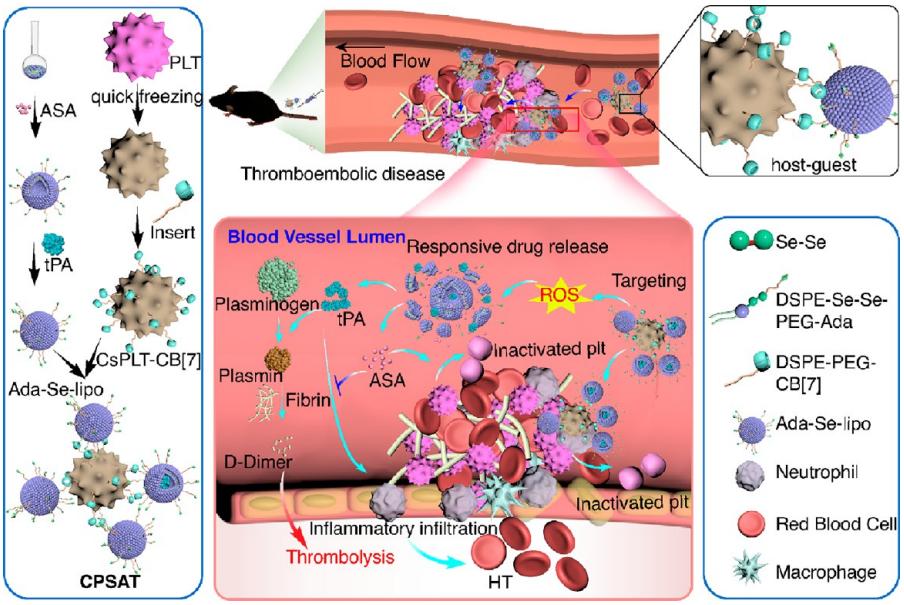

[a]After platelets were isolated and activated with thrombin, cryo-shocked platelets were obtained by quick freezing methods. DSPE-PEG-CB [7] were decorated on the surface after incubation to prepare the CB [7] modified cryo-shocked platelets (CsPLT-CB [7]). Amantadine crosslinked ROS-responsive liposomes (Ada-Se-lipo) were synthesized and conjugated to CsPLT-CB [7] via CB[7]-Ada host−guest interaction. Attributed to the guidance of special receptors on the surface, CPSAT could effectively target thrombus sites. Moreover, occupation of receptors on activated platelets by cryo-shocked platelets antagonized further activation of circulating resting platelets. Thrombolytic tPA and anti-inflammatory aspirin released rapidly under the stimulation of high-level ROS during thrombosis. Aspirin inhibited tPA-induced inflammatory infiltration and reduced the risks of hemorrhage transformation (HT). Furthermore, effectively accumulation, occupation of activated platelets receptors inhibited platelets further to be activated, and responsive released tPA enhanced thrombolytic efficacy and anti-inflammatory aspirin reversed tPA treatment induced hemorrhage transformation, exerting the powerful therapeutic efficacy of CPSAT on thromboembolic disease.

neutrophil extracellular traps (NETs).[16] On the other hand, the only Food and Drug Administration (FDA)-approved thrombolytic drug for thromboembolic disease, tissue plasminogen activator (tPA), has shown powerful thrombolytic efficacy within 4.5 h of disease occurrence in clinics; however, the narrow therapeutic time window and high risks of hemorrhage transformation (HT) have limited its widespread application.[17,18] Although the administration of ASA alone is impossible for acute thromboembolic disease treatment, the potential inhibitory effect of tPA-induced neutrophil infiltration by ASA remains to be explored.

Nanomaterials were extensively explored to enhance the targeted delivery of antithrombotic drugs, such as liposomes,[19] solid lipid nanoparticles,[20] polymer-based nanoplatforms,[21,22] responsive nanoparticles,[23,24] and biomimetic nanoparticles.[25] Inorganic nanoparticles, especially mesoporous silica nanoparticles, were outstanding for their high surface area, controllable framework composition, and mesoporous structure, and they showed great potential in imaging and treatment of thrombus-related diseases.[26] However, the unavoidable formulation of a protein corona on the surfaces of a particle after exposure to biological milieu and the lack of standardized toxicity assessment methods as well as the requirement of additional targeting modification need to be addressed to accelerate the clinical transformation.[27] Biomimetic nanomedicines, with enhanced immune compatibility, safety, and targeting efficiency, were developed rapidly in the most recent decade for improved targeting;[28] nevertheless, the targeting efficiency still has room for improvements. In addition, microenvironment-responsive nanomedicines showed their advantages, which not only reduced the "PEG dilemma" (PEG = poly(ethylene glycol)) but also enhanced specificity and therapeutic efficacy.[29] A study showed that biomimetics coupled with ROS-responsive nanomedicine also achieved decent efficacy against inflammatory microglia polarization after ischemic stroke.[30]

Over the years, cell-based therapy is an emerging therapeutic strategy with the potential to treat refractory disease due to its high targeting efficiency to specific tissues, in response to relevant pathological signals and local microenvironment.[31] As an indispensable component of blood, platelets are apt to aggregate at a thrombus site.[32] Infusion of platelets is primarily applied to hemostasis, inflammatory reactions, and promoting wound healing; nevertheless, the limited shelf life of platelets and ease of activation have restricted its extended application and produced a large amount of waste.[33] In recent years, a platelet-based drug delivery platform has attracted increasing attention due to its powerful thrombus targeting, injured vessels binding, and immune compatibility.[34] However, a live platelet has the potential risk of inducing thrombosis due to the ease of activation, which indeed is one of the adverse reactions after platelet transfusion.[35] To overcome the defects of live platelets and potentially recycle cryopreserved platelets, meanwhile, inspired by the cryo-shocked tumor cells-based drug delivery and vaccination system,[36] we investigated the potential of cryo-shocked, preactivated platelets for targeted therapy of thromboembolic disease.

Herein, a cryo-shocked platelet-based drug delivery system was developed, via noncovalent conjugation of cryo-shocked platelets (CsPLTs) and drug-loaded ROS-responsive liposomes

https://doi.org/10.1021/acsnano.2c11865
ACS Nano 2023, 17, 6519−6533

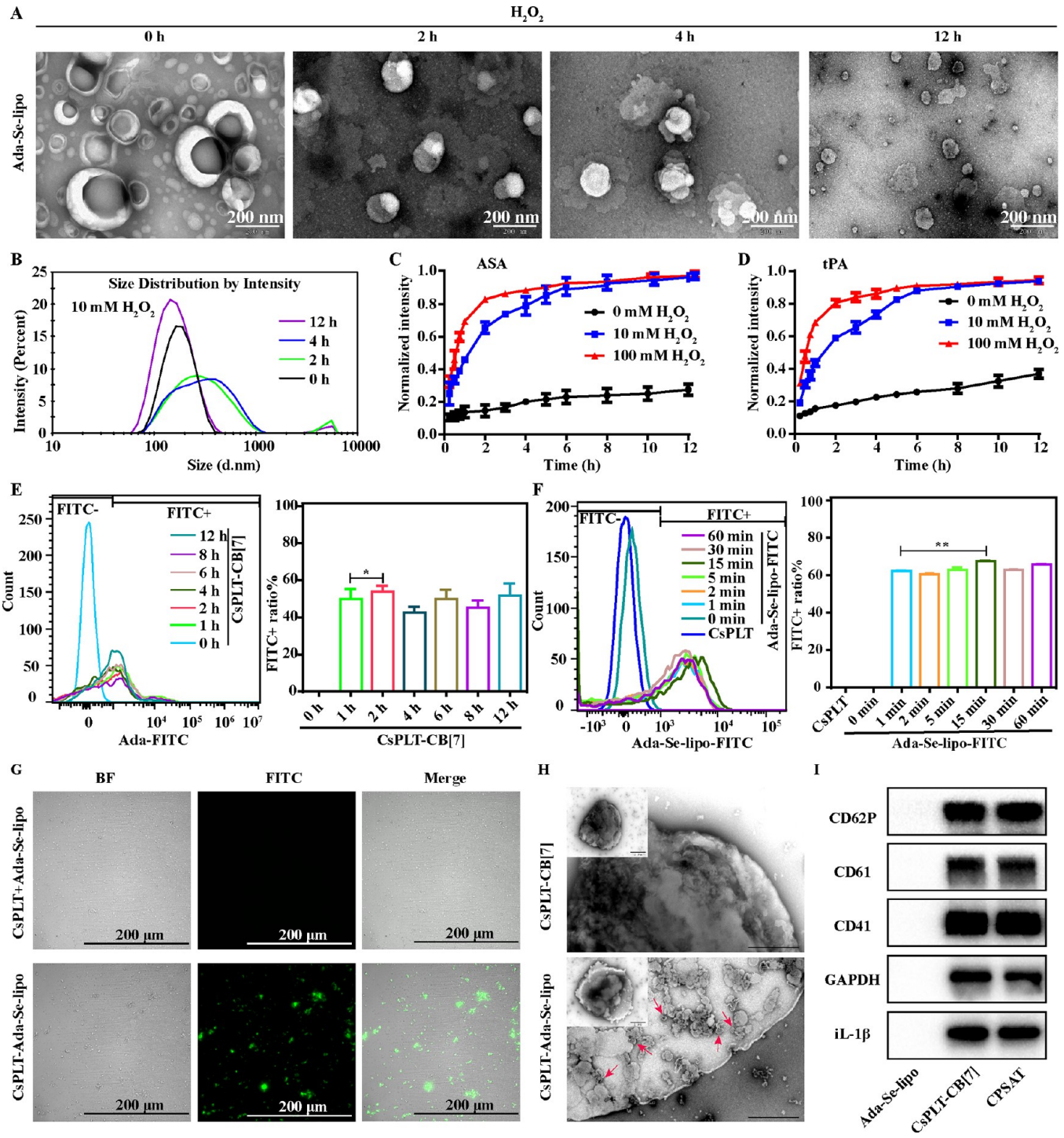

Figure 1. Preparation and characterization of Ada-Se-lipo, CsPLT-Ada-Se-lipo, and CPSAT. (A) Representative TEM images of Ada-Se-lipo with H_2O_2 (10 mM) after incubation for 0, 2, 4, and 12 h, respectively. Scale bar: 200 nm. (B) The typical hydrodynamic diameters of Ada-Se-lipo after incubation with H_2O_2 (10 mM) for 0, 2, 4, and 12 h, respectively. (C, D) Drug release profile of ASA and tPA from ASAT after incubating with H_2O_2 (0, 10, and 100 mM) last for 12 h in vitro. (E) Representative histogram and qualitative analysis of CsPLT measured by flow cytometry, after incubation with DSPE-PEG-CB [7] for 0, 1, 2, 4, 6, 8, and 12 h, respectively. (F) Representative histogram and qualitative analysis of Ada-Se-lipo-FITC by flow cytometry, after incubation with CsPLT-CB [7] for 0, 1, 2, 5, 15, 30, and 60 min, respectively. CsPLT incubated with Ada-Se-lipo-FITC for 15 min served as a negative control. (G) Representative fluorescent CLSM images of CsPLT and CsPLT-CB [7] incubated with Ada-Se-lipo-FITC for 15 min. Scale bar: 200 μm. (H) Representative TEM images of CsPLT-CB [7] and CsPLT-Ada-Se-lipo after incubation with Ada-Se-lipo-FITC for 15 min. Scale bar: 500 nm. (I) Typical proteins in platelet membrane and cytoplasm detected in Ada-Se-lipo, CsPLT-CB [7], and CPSAT, respectively. All data were presented as mean ± SD. (n = 3). *$P \leq 0.05$, **$P \leq 0.01$, ***$P \leq 0.001$, or ****$P \leq 0.0001$.

(Scheme 1). In the design, preactivated platelets were cryo-shocked via a liquid nitrogen-based quick freezing method to prepare CsPLTs. These platelets maintained most of the entire platelet structure and morphology and retained all surface

https://doi.org/10.1021/acsnano.2c11865
ACS Nano 2023, 17, 6519−6533

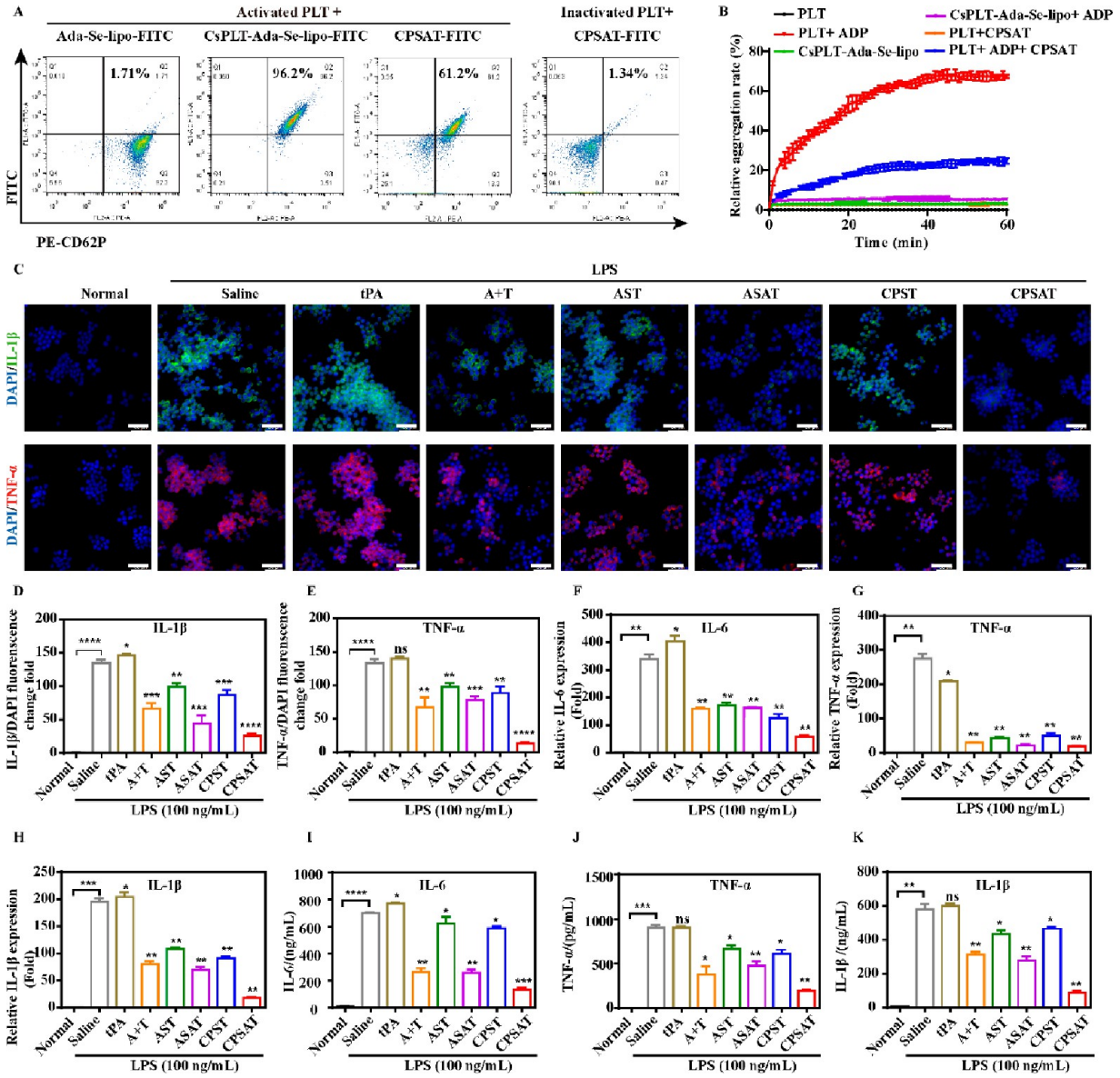

Figure 2. In vitro binding to activated platelets, antiactivation platelets, and anti-inflammation effect of CPSAT. (A) Typical plots of the combination of FITC-labeled Ada-Se-lipo, CsPLT-Ada-Se-lipo, and CPSAT with PE-labeled activated platelets and inactivated platelets, respectively. (B) Aggregation assay of platelets after incubation with CPSAT under the stimulation of thrombin and calcium. (C) Immunofluorescent staining of IL-1β and TNF-α in LPS-stimulated RAW264.7 cells after incubation with Saline, tPA, A+T, AST, ASAT, CPST, and CPSAT. Scale bar: 50 μm. (D, E) Relative fluorescence analysis on the expressions of IL-1β and TNF-α in (C). (F−H) Relative mRNA expressions of IL-6, TNF-α, and IL-1β in LPS-stimulated RAW264.7 cells after different treatments for 12 h. (I−K) The concentrations of IL-6, TNF-α, and IL-1β in LPS-stimulated RAW264.7's supernatant after different treatments for 12 h. All data were presented as mean ± SD. (n = 3). *$P \leq 0.05$, **$P \leq 0.01$, ***$P \leq 0.001$, and ****$P \leq 0.0001$.

proteins allowing for thrombus targeting. Cucurbit[7]uril (CB[7])-decorated, cryo-shocked, preactivated platelets, named CsPLT-CB [7], were prepared to conjugate with adamantane (Ada)-modified drug loaded, ROS-responsive liposome, mediated via CB[7]-Ada host−guest interactions. Both tPA and ASA were encapsulated in liposomes. In thromboembolic disease mouse models, the supramolecularly engineered cryo-shocked cell-based delivery system showed powerful thrombus-targeting and excellent therapeutic efficacy.

RESULTS AND DISCUSSION

Preparation and Characterization of CPSAT. To prepare cryo-shocked platelets (CsPLTs), platelets were extracted from C57BL/6J mice blood with a low-speed centrifuge method and suspended in cryopreservation buffer after activation, followed with being frozen in liquid nitrogen for at least 12 h. Platelets presented high expressions of platelet activation markers CD62P and phosphatidylserine on the surface as well as cryopreservation-enhanced CD62P[37−40] (Figure S1A−C). After cryo-shock, the percent of dead platelets was up to 85% (Figure S1D−F), affording dead and CD62P- and phosphatidylserine-over-exposed microcarriers. The CsPLT exhibited a rougher surface than that of freshly isolated platelets under scanning electron microscopy (SEM) (Figure S2A). Coomassie brilliant blue staining and Gene Ontology Annotation analysis revealed the preservation of platelet proteins before and after being cryo-shocked (Figure S2B,C), and the typical proteins, IL-1β,

https://doi.org/10.1021/acsnano.2c11865
ACS Nano 2023, 17, 6519−6533

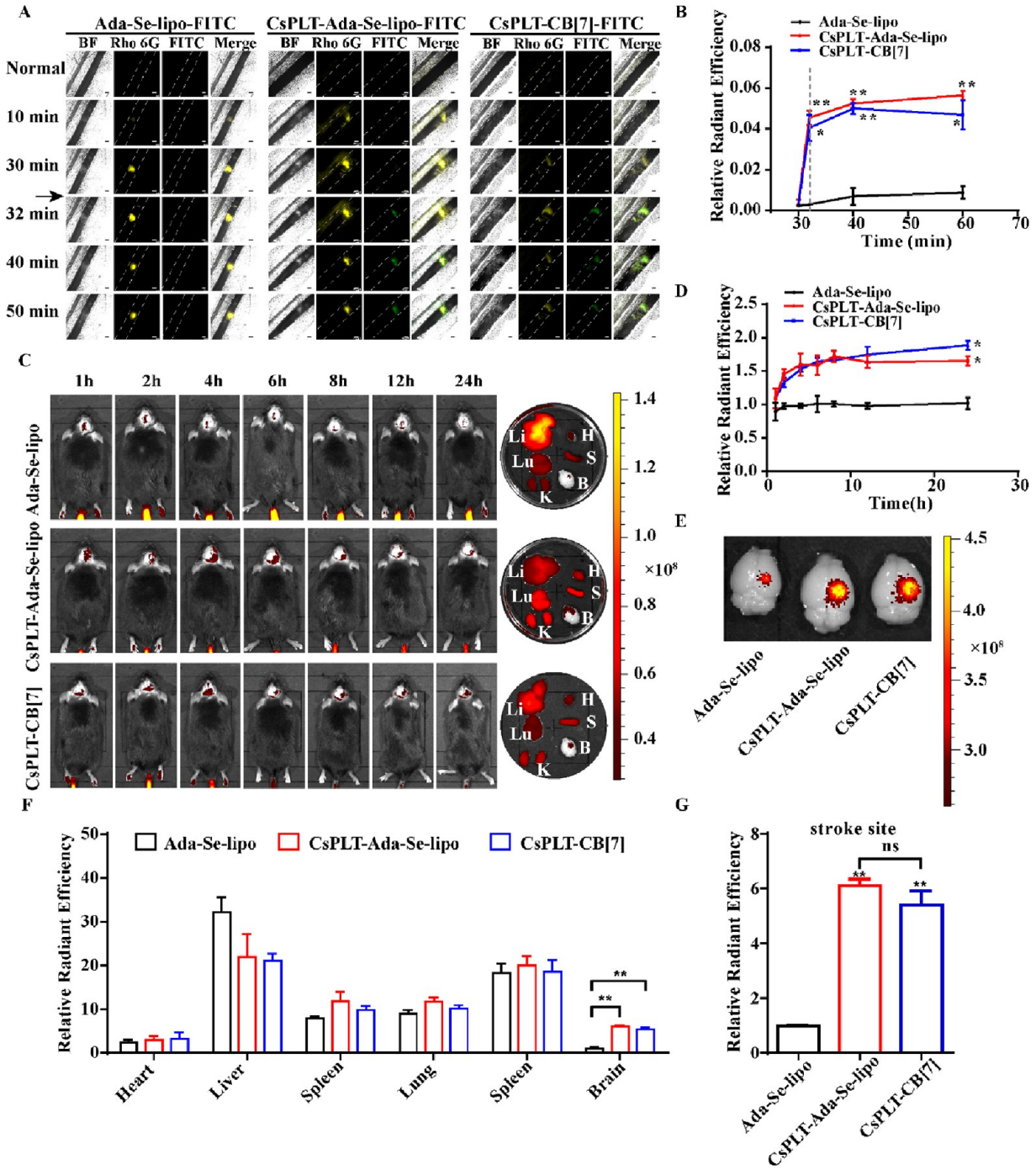

Figure 3. Thrombus targeting of CsPLT-Ada-Se-lipo in mesenteric thrombosis and acute stroke models. (A) Thrombus-targeting by FITC-labeled Ada-Se-lipo, CsPLT-Ada-Se-lipo, or CsPLT-CB [7], after platelets labeled by Rho6G (scale bar: 100 μm). (B) Quantification of the FITC intensity in thrombus site at various time points in (A). (C) In vivo biodistribution of Cy5.5-labeled Ada-Se-lipo, CsPLT-Ada-Se-lipo, or CsPLT-CB [7] after various durations. Abbreviation representatives; Li: Liver, S: Spleen, Lu: Lung, B: Brain, H: Heart. (D) Relative fluorescence intensity changes of Cy5.5-labeled Ada-Se-lipo, CsPLT-Ada-Se-lipo, or CsPLT-CB [7] in cerebral infarction for various durations. (E) Typical images of the fluorescence efficiency in the brain at 24 h after injection. (F) Quantitative analysis on the fluorescence intensity of major organs after administration for 24 h in stroke mice. (G) Quantitative analysis on the relative fluorescence intensity in stroke sites of (E). All data were presented as mean ± SD. (n = 3). *$P \leq 0.05$, **$P \leq 0.01$, ***$P \leq 0.001$, or ****$P \leq 0.0001$.

GAPDH, CD41, CD61, and CD62P, were well-retained (Figure S2D). Besides, the targeting efficiency of cryo-shocked platelets in a stroke site was lower than that of living activated platelets (Figure S2E−G). However, the dead platelets due to cryo-shock, as well as the occupation of activated platelet receptors by cryo-shocked platelets, prevented these platelets from further activation in circulation, leading to potentially stable, safe antithrombosis in vivo (Figure S2H). Furthermore, the risk of inducing thrombosis by cryo-shocked platelets was directly confirmed to be very low, when compared with those by saline and native platelets via quantitative analysis for infarction volume (Figure S2I).

Next, an amantadine-modified, PEGylated, ROS-responsive liposome (Ada-Se-lipo) was synthesized by a thin-film hydration

https://doi.org/10.1021/acsnano.2c11865
ACS Nano 2023, 17, 6519−6533

method with DSPE−Se−Se-PEG-Ada (DSPE = 1,2-distearoyl-sn-glycero-3-phosphoethanolamine), derived from DSPE−Se−Se-PEG-NHS and Ada-NH_2 via an ester−amide reaction (Figure S3). Transmission electron microscopy (TEM) analysis showed the typical bilayer structure of liposome with a diameter of 162.3 ± 2.8 nm (Figure 1A,B). As expected, the morphology and size distribution of Ada-Se-lipo changed after treatment with 10 mM H_2O_2 for 0, 2, 4, and 12 h, respectively (Figure 1A,B), as a result of ROS-responsiveness.[41] To prepare the ASA- and tPA-loaded Ada-Se-lipo (ASAT), ASA was added during the film preparation; meanwhile, tPA was freshly dissolved in the hydration buffer. Encapsulation efficiency (EE) and drug loading capacity (LC) were calculated (Table 1); the EE and LC of ASA were up to 84.1% and 7.7%, respectively, and the EE and LC of tPA in ASAT were 30.3% and 1.95%, respectively. Over 80% ASA and tPA inside liposomes were rapidly released into the incubation solution within 6 h (Figure1C,D) in the presence of 0, 10, and 100 mM H_2O_2. The stability of Ada-Se-lipo and ASAT within 7 days was verified by monitoring the size distribution and Zeta potential (Figure S4).

CB [7]-decorated CsPLT, namely, CsPLT-CB [7], was obtained via a ligand-insertion approach with DSPE-PEG-CB [7].[42] The concentration of CB [7] on platelets was quantified to be approximately 0.1×10^{-7} μM CB [7] per CsPLT, based on an inductively coupled plasma−mass spectrometry (ICP-MS) analysis of a metal-containing guest oxaliplatin.[43] Previously, CB [7] anchored on a macrophage could be eliminated within several hours, ascribed to the fluidity of the membrane and phagocytosis of the macrophage.[42] In the current work, as shown in Figure 1E, CsPLT-CB [7] was facilely obtained via incubation of the cells with DSPE-PEG-CB [7] for 2 h, and the host molecule was stable on the surface of platelets for at least 16 h (Figure S5), likely due to the low fluidity of the CsPLT membrane after cryo-shock, beneficial to the long-term preservation. Meanwhile, the anchored CB [7] on the surface of CsPLT-CB [7] did not impact the targeting efficiency of CsPLT to ischemic stroke sites (Figure S6).

CsPLT-Ada-Se-lipo was fabricated by mixing CsPLT-CB [7] with Ada-Se-lipo for different durations (15 min seemed sufficient) (Figure 1F). Confocal laser scanning microscopy (CLSM) images in Figure 1G and TEM images in Figure 1H manifested the successful preparation of CsPLT-Ada-Se-lipo, with the quantification of Ada-Se-lipo on the surface of each cryo-shocked platelet being about 35.28 ± 2.53 pg (Figure S7). After successfully encapsulating ASA and tPA into CsPLT-Ada-Se-lipo, the cryo-shocked platelet-based cell-hitchhiking drug delivery system (CPSAT) was obtained, with the EE and LC of ASA being 83.5% and 5.2% and the EE and LC of tPA being 29.6% and 1.23%, respectively (Table 1). A western blot analysis of platelet proteins, IL-1β, GAPDH, CD41, CD61, and CD62P, on the Ada-Se-lipo, CsPLT-Ada-Se-lipo, and CPSAT, suggested the preservation of the surface proteins in the supramolecularly engineered CsPLT (Figure 1I).

In Vitro Binding, Antiactivation Platelets, and Anti-Inflammation of CPSAT. Binding of Ada-Se-lipo, CsPLT-Ada-Se-lipo, and CPSAT to activated platelets was analyzed via flow cytometry. Activated platelets were distinguished with PE-labeled CD62P, a typical marker of platelet activation status, and the combination of FITC-labeled Ada-Se-lipo, CsPLT-Ada-Se-lipo, or CPSAT with activated platelets was assessed after incubation for 15 min. CsPLT-Ada-Se-lipo showed the strongest binding to activated platelets, whereas Ada-Se-lipo failed to bind activated platelets (Figure 2A, Figure S8A). However, the decreased binding of CPSAT to activated platelets was observed, when compared with the CsPLT-Ada-Se-lipo group, likely attributed to the antagonistic effect of the loaded ASA. Subsequently, the antiactivation effect of CPSAT toward platelets was verified after coincubation for 30 min (Figure S8B). The platelets aggregation rate (triggered with ADP) was significantly inhibited by CPSAT, suggesting the safety of CPSAT (Figure 2B). The binding and inhibition of CPSAT to inactivated platelets were rather limited, possibly due to the lack of specific ligands in inactivated platelets, which are mainly expressed in activated platelets. To confirm this hypothesis, inhibitors and antibodies were, respectively, used to antagonize the receptors in fluorescein isothiocyanate (FITC)-labeled CPSAT for 15 min; the combination with PE-labeled activated platelets was significantly decreased, especially in GPIIb/IIIa, CD61, and CD62P antagonized groups (Figure S9). These observations suggest the significant potential of CPSAT in targeting platelet-rich thrombosis. To predict the anti-inflammation efficacy after preparation of the drug delivery system, RAW264.7 cells were incubated with lipopolysaccharide (LPS) and subsequently treated with saline, tPA, ASA + tPA (A + T), AST (tPA@ Ada-Se-lipo), ASAT (tPA/ASA@ Ada-Se-lipo), CPST (tPA@ CsPLT-Ada-Se-lipo), and CPSAT (tPA/ASA@ CsPLT-Ada-Se-lipo) for 12 h, respectively. As shown in Figure 2C−E, CPSAT inhibited the significantly increased levels of TNF-α and IL-1β. The mRNA expressions of IL-6, TNF-α, and IL-1β in RAW 264.7 cells were dramatically decreased by CPSAT (Figure 2F−H). Accordingly, the concentrations of expressed IL-6, TNF-α, and IL-1β in culture supernatant were also inhibited (Figure 2I−K). CPSAT obviously exhibited the anti-inflammatory activity, mainly due to the anti-inflammatory activity of aspirin. In addition, the ROS-responsive selenium also contributed to the anti-inflammatory effect, as suggested by previous reports.[44]

In Vivo Targeting of CsPLT-Ada-Se-lipo to Thrombus. To examine the applicability of CsPLT-CB [7] and CsPLT-Ada-Se-lipo in vivo, a visible mesenteric artery thrombosis mice model was first established by $FeCl_3$-induced damage of endothelial cells. In this study, 100 μL of Rho 6G was injected to label the platelets in vivo before the disease model was established, and the stable thrombus was formulated after incubation for 30 min. FITC-labeled Ada-Se-lipo, CsPLT-Ada-Se-lipo, and CsPLT-CB [7] were injected within 2 min after thrombosis for real-time fluorescence microscopic monitoring at 32, 40, and 50 min after injection. CsPLT-Ada-Se-lipo and CsPLT-CB [7] exhibited efficient targeting to thrombus in comparison to Ada-Se-lipo (Figure 3A,B). Next, we investigated the biodistribution of Cy5.5-labeled Ada-Se-lipo, CsPLT-Ada-Se-lipo, and CsPLT-CB [7] in stroke mice model within 24 h after administration. CsPLT-Ada-Se-lipo and CsPLT-CB [7] efficiently accumulated in cerebral infarction lesion, while Ada-Se-lipo showed a low level of aggregation (Figure 3C,D). Harvested mice brains' images showed the efficient targeting of CsPLT-Ada-Se-lipo and CsPLT-CB [7] to the thrombus, and the modification of CB [7] and Ada-Se-lipo showed little interference on thrombus targeting of CsPLT (Figure 3E and Figure S6). Ex vivo fluorescence analysis further confirmed the long retention of CsPLT-Ada-Se-lipo in the stroke sites, and the fluorescence intensity of stroke brain was increased to 6-fold after administration for 24 h (Figure 3F,G). These results indicated the successful in vivo targeting to thrombosis sites of CsPLT-Ada-Se-lipo, and the anchored Ada-Se-lipo did not interfere the targeting efficiency of CsPLT.

https://doi.org/10.1021/acsnano.2c11865
ACS Nano 2023, 17, 6519−6533

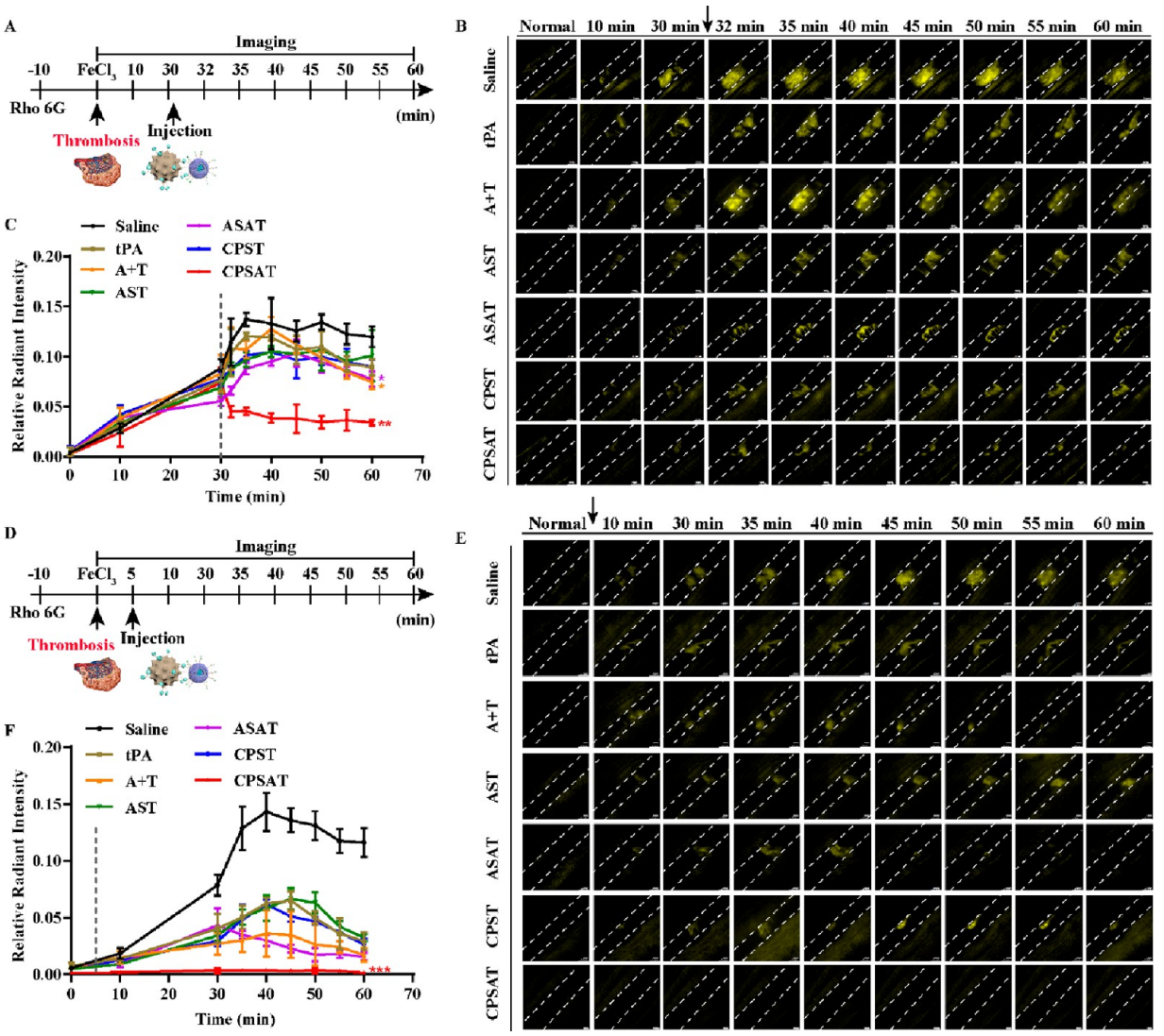

Figure 4. Therapeutic efficiency of CPSAT in mesenteric thrombosis model. (A) Scheme of the treatment process in mesenteric thrombosis model after thrombus formation. (B) Typical images of thrombolysis in mice treated by saline, tPA, A+T, AST, ASAT, CPST, and CPSAT after formation of visible thrombus. (C) The relative fluorescence quantification of thrombus site at various times in (B) (n = 3). (D) Scheme of the preventive treatment process in mesenteric thrombosis mouse model before thrombus formation. (E) Typical images of thrombolysis by saline, tPA, A+T, AST, ASAT, CPST, and CPSAT before the formation of visible thrombus. (F) The relative fluorescence quantification of thrombus site at various time points in (E) (n = 3) (scale bar: 100 μm). All data were presented as mean ± SD. *$P \leq 0.05$, **$P \leq 0.01$, ***$P \leq 0.001$, and ****$P \leq 0.0001$.

In Vivo Thrombolytic Efficacy in Mesenteric Artery Thrombosis Model. Therapeutic efficacy of CPSAT in visualized thrombosis model was evaluated. For thrombolysis analysis, saline, tPA, ASA + tPA (A + T), AST (tPA@ Ada-Se-lipo), ASAT (tPA/ASA@ Ada-Se-lipo), CPST (tPA@ CsPLT-Ada-Se-lipo), and CPSAT (tPA/ASA@ CsPLT-Ada-Se-lipo) were injected, respectively, after thrombus formation at 30 min, as shown in Figure 4A. The fluorescence intensity of thrombus in CPSAT-treated mice disappeared quickly during 30 min monitoring after administration, suggesting the powerful thrombolytic efficiency of CPSAT on platelet-rich thrombus in culprit vessels (Figure 4B,C). To explore the potential preventive actions of thrombosis, saline, tPA, A+T, AST, ASAT, CPST, and CPSAT were injected at 5 min before formation of thrombus, as shown in Figure 4D. Accordingly, CPSAT significantly delayed the thrombosis duration (Figure 4E,F). Additionally, ASA and CsPLT-Ada-Se-lipo also showed moderate thrombolytic efficacies as shown in Figure S10.

In Vivo Thrombolytic Efficacy in Ischemic Stroke Model. Subsequently, a photochemically induced ischemic stroke mice model was established to assess the therapeutic efficacy of CPSAT. The therapeutic procedure and corresponding indicators analysis were shown in the scheme (Figure 5A). Before the experiment, all animals were trained for Catwalk XT system. After establishment of the model, mice were divided into seven groups, saline, tPA, A+T, AST, ASAT, CPST, and CPSAT, and were intravenously injected, respectively, after photochemically induced stroke for 1.5 h; meanwhile, the sham group was regarded as a negative control without laser irradiation. Mice brains were imaged at 48 h postadministration by magnetic resonance imaging (MRI), laser speckle imaging (LSI), and optical coherence tomography (OCT), respectively. As shown in Figure 5B,F, the CPSAT-treated group obviously decreased

https://doi.org/10.1021/acsnano.2c11865
ACS Nano 2023, 17, 6519−6533

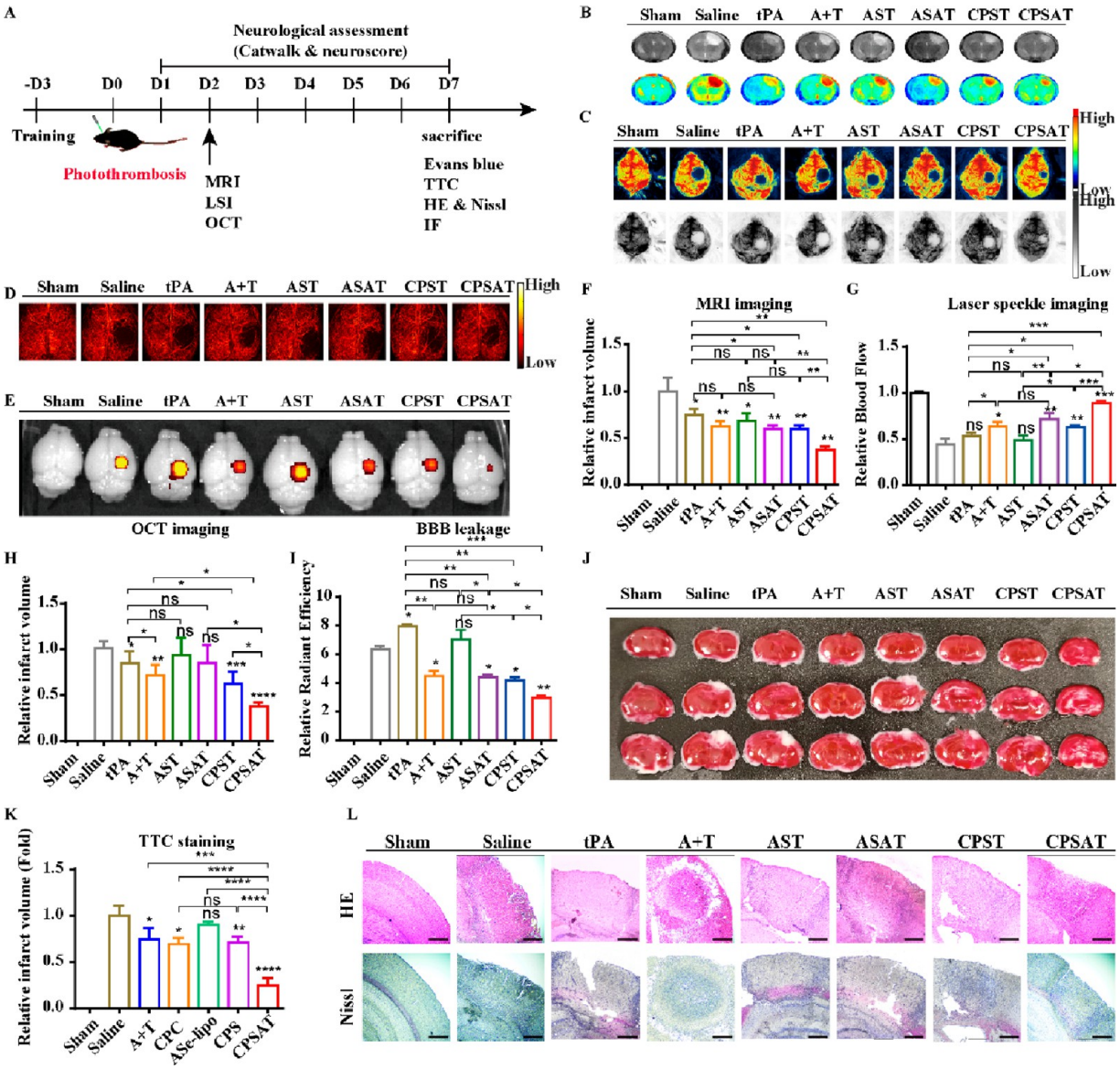

Figure 5. Therapeutic efficacy of CPSAT in acute stroke mouse model. (A) Schematic diagram of the therapeutic procedure in acute stroke mice (n = 12). (B) Typical MRI images at 48 h postadministration were shown (n = 3). (C) Typical laser speckle images of the relative blood flow at 48 h postadministration were conducted (n = 3). (D) Typical OCT images of infarct volume at 48 h postadministration were measured (n = 3). (E) Representative Evans Blue leakage images of BBB at 7-day postadministration were exhibited (n = 3). (F−I) Quantitative analysis of typical MRI images, laser speckle images, OCT images, and Evans Blue leakage images at (B−E), respectively. (J−K) Typical TTC staining images and quantitation of stroke volume at 7-day were employed (n = 3). (L) Representative images of H&E and Nissl staining in infarct volume at 7-day postadministration (n = 3) (scale bar, 100 μm). All data were presented as mean ± SD. *$P \leq 0.05$, **$P \leq 0.01$, ***$P \leq 0.001$, or ****$P \leq 0.0001$.

the infarct volume and restored the blood flow recanalization that was blocked by thrombosis, as was reflected by the LSI outcomes (Figure 5C,G) and OCT images (Figure 5D,H). Meanwhile, CPSAT also exhibited protective effects on the blood-brain barrier (BBB) integrity (Evans Blue leakage), which was considered essential to maintain the brain health (Figure 5E,I). Figure S11 showed the relatively low therapeutic efficacy in the stroke model. At the end point, major organs were collected after mice were sacrificed, including brain, lung, heart, spleen, kidney, and liver. The cerebral infarct area in stroke mice was measured by staining with 2,3,5-triphenyltetrazolium chloride (TTC) after brains were sliced. The staining results suggested the powerful curative effect of CPSAT due to the high targeting efficiency and the anti-inflammation effects (Figure 5J,K). H&E and Nissl staining images further attested the significant therapeutic efficacy of CPSAT (Figure 5L). Fibrin degradation products (FDPs) are some small pieces produced in blood after thrombolytic treatment, typically used to evaluate the blood clots, stroke, and heart disease. In our study, the most common type of FDPs, D-dimer, was detected to assess the ability of fibrin degradation, which was significantly decreased by CPSAT after administration for 7 days (Figure S12).

To appraise the efficacy and monitor the safety of CPSAT during the treatment, a neurological assessment was conducted by modified neurological severity scores (mNSS) and Catwalk XT each day, accordingly to previously reported approaches.[45] In contrast with other treatment groups, the CPSAT-treated mice had a much lower score, reflecting the alleviation of neurological deficits that resulted from stroke (Figure 6A−C, Table 2). No pathological abnormality in major organs reflected

https://doi.org/10.1021/acsnano.2c11865
ACS Nano 2023, 17, 6519−6533

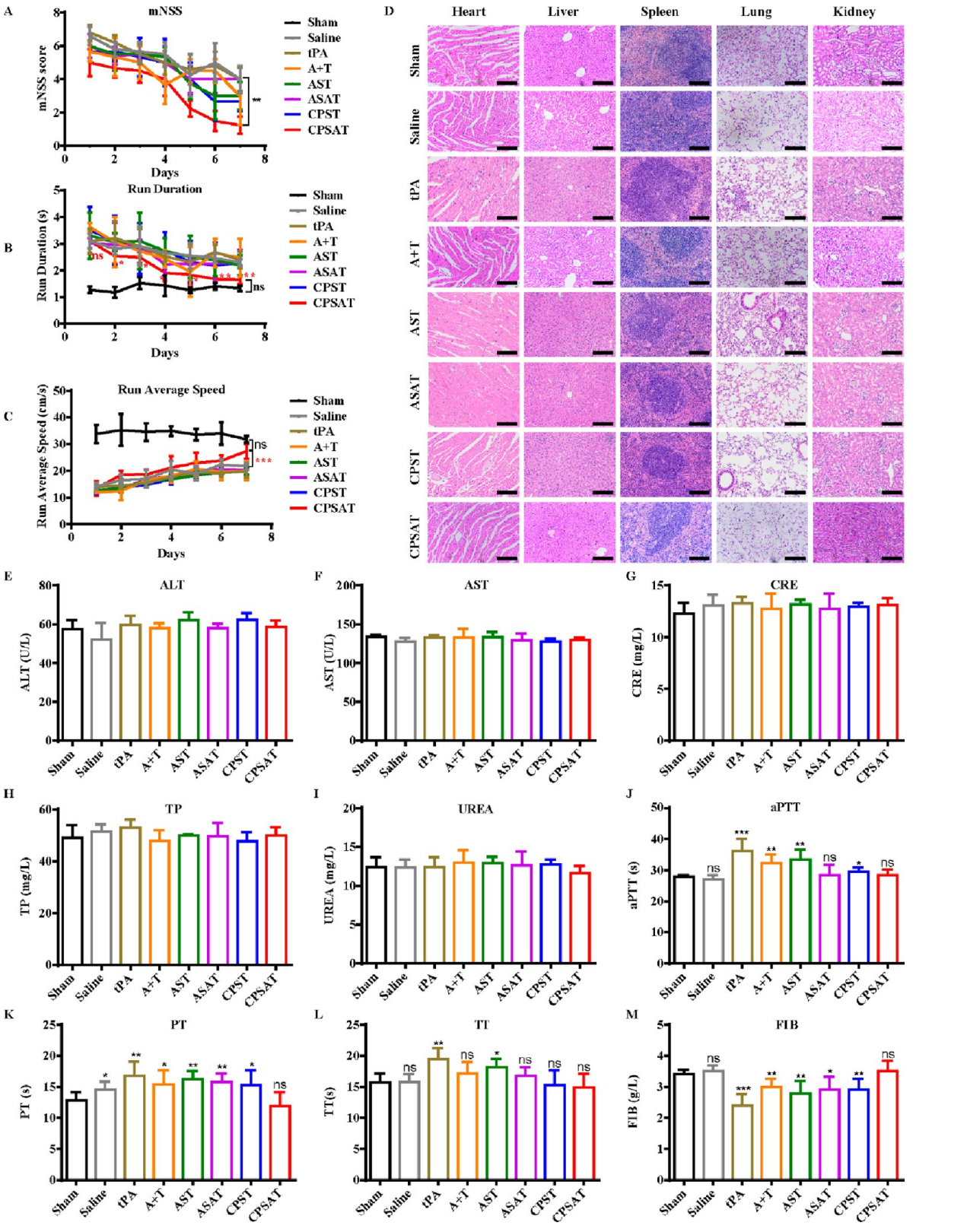

Figure 6. Evaluation of neurological functions and safety profiles after a 7-day administration of CPSAT in acute stroke. (A) The mNSS of the sham, saline, tPA, A+T, AST, ASAT, CPST, and CPSAT treated groups, respectively. (B) Run duration and run average speed (C) of sham, saline, tPA, A+T, AST, ASAT, CPST, and CPSAT treated groups, respectively. (D) H&E staining images of organs in saline, tPA, A+T, AST, ASAT, CPST, and CPSAT treated mice, respectively. (Scale bar, 100 μm). (E−I) Typical indicators of liver (ALT and AST) and kidney function (CRE, TP, and UREA) in treated mice. (J−M) Coagulation indicators (aPTT, FIB, PT, and TT) postinjection with saline, tPA, A+T, AST, ASAT, CPST, and CPSAT, respectively ($n = 6$). All data were presented as mean ± SD. *$P \leq 0.05$, **$P \leq 0.01$, ***$P \leq 0.001$, or ****$P \leq 0.0001$ (All groups compared with saline-treated group).

https://doi.org/10.1021/acsnano.2c11865
ACS Nano 2023, 17, 6519−6533

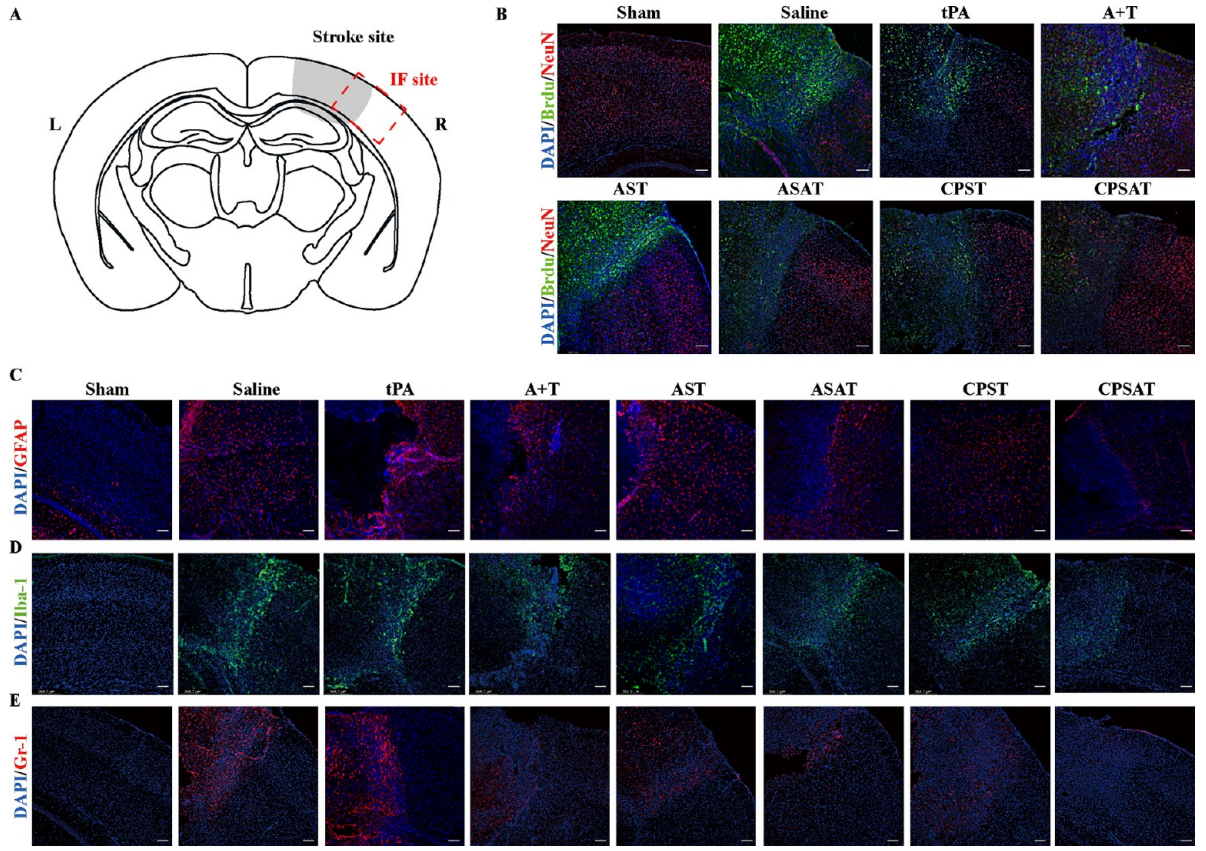

Figure 7. Suppression of reactive glial cells, inflammatory cells infiltration in CPSAT-treated infarction poststroke. (A) Schematic of the immunofluorescence (IF) staining site in stroke brain. L: left, R: right. (n = 3). (B) Representative IF images of Brdu (green, apoptosis cells) and NeuN (red, neurons). Scale bar: 100 μm. (C−E) Representative IF images of glial fibrillary acidic protein (GFAP) staining (red, astrocytes), ionized calcium binding adapter molecule 1 (Iba-1) staining (green, microglial/macrophage), and Gr-1 (red, infiltration of neutrophil), respectively. Scale bar: 100 μm.

the safety of this formulation (Figure 6D). Liver (ALT and AST, Figure 6E,F) and kidney functions (CRE, TP, and UREA, Figure 6G−I) as well as the blood coagulation parameters (aPTT, PT, TT, and FIB) (Figure 6J−M) of CPSAT-treated mice were comparable with those of the sham group, further attesting to the decent safety profile of this formulation.

In Vivo and In Vitro Action Mechanisms of CPSAT. Astrocyte serves an irreplaceable role in the regulation of BBB permeability and maintenance of cerebral blood flow.[46−48] Astrocyte activation that occurred during the damage and repair of a neurovascular unit poststroke participates in the process of glial scar formation, which is generally considered detrimental to neurite outgrowth and axonal regeneration.[49,50] Suppression of reactive astrogliosis contributes to the neurological recovery, suggesting the necessity of antiactivation of astrocyte.[51] Microglia and circulating macrophage polarization occurs poststroke, and antiactivation of microglia/macrophages helps to reduce the inflammatory injuries in the early stage.[52] Therefore, immunofluorescence staining of infarction was conducted, and the results (Figure 7A) demonstrated the lower cellular apoptosis (BrdU) and higher neuronal (NeuN, neuron marker) survival after CPSAT administration (Figure 7B, Figure S13A,B). Besides, the reduced GFAP expression in astrocytes indicated the suppression of reactive astrogliosis after treatment with CPSAT, when compared those treated with tPA and others (Figure 7C, Figure S13C). Ionized calcium binding adapter molecule 1 (Iba-1), exclusively expressed in activated microglial and macrophage, showed significant growth after ischemic stroke. CPSAT treatment dramatically restrained the increase of Iba-1 (Figure 7D, Figure S13D). In addition, tPA treatment induces HT by enhancing the neutrophils infiltration.[18] Therefore, we evaluated the activity of recruited neutrophils in infarction by analyzing the expression of granulocyte receptor-1 (Gr-1).[53] As shown in Figure 7E and Figure S13E, CPSAT treatment inhibited the neutrophil recruitment. All these anti-inflammation effects were mostly attributed to the anti-inflammatory activity of ASA (Figure S14). Collectively, all these results demonstrated the superior therapeutic effect of CPSAT against stroke in mice and suggested its significant potential for clinical translation.

CONCLUSIONS

In the study, we designed and prepared a cryo-shocked cell-based drug delivery system comprising of cryo-shocked platelets and tPA and ASA coloaded ROS-responsive liposomes, mediated via host−guest interaction. The system exhibited a high thrombus-targeting efficiency and thrombolytic and anti-inflammation effects in vitro and in vivo within thromboembolic disease mice models. The excellent targeting efficiency to thrombi was attributed to the thrombus tropism of preactivated platelets. Under the guidance of CsPLT and the stimulation of ROS, tPA and ASA were released locally in the thrombus site, exerting the thrombolytic effect and anti-inflammation activity. The mechanisms of therapeutic action in ischemic stroke mice administered with CPSAT were on account of the suppression of reactive astrogliosis, inhibition of microglial or macrophage

https://doi.org/10.1021/acsnano.2c11865
ACS Nano 2023, 17, 6519−6533

polarization, and obstruction of the enhanced neutrophil infiltration caused by tPA treatment, which contributed to the amelioration of neurological function. Hence, anti-inflammatory ASA effectively exhibited antiactivation activity of platelets and inhibited the excessive inflammatory infiltration of macrophage and neutrophil enhanced by tPA administration, further reducing the risk of hemorrhagic transformation. Our study not only provides a safe thrombus-targeting cryo-shocked nonliving platelet-hitchhiking tPA/ASA delivery system for a highly effective thromboembolic disease treatment but also proposes a brief methodology to reuse cryopreserved platelets and reduce associated wastes.

MATERIALS AND METHODS

Materials and Reagents. 1,2-Distearoyl-*sn*-glycero-3-phosphoethanolamine−Se-Se-(poly(ethylene glycol))-NHS (DSPE−Se−Se-PEG-NHS) was purchased from Xi'an Ruixi Biological Technology Co., Ltd. (China). DSPE-PEG-CB [7] was synthesized by DSPE-PEG-SH and monoallyloxy CB [7] synthesized in our laboratory according to our previous procedure. Soybean lecithin, cholesterol, and all other chemical reagents were obtained from Shanghai Aladdin Biochemical Technology Co., Ltd. (China).

Acetylsalicylic acid (ASA) was purchased from (DRE-C10024000) Dr. Ehrenstorfer GmbH (Germany). Tissue plasminogen activator (t-PA, Alteplase) was acquired from Boehringer Ingelheim Pharma GmbH & Co. KG. And the activity assay kit of tPA was received from BioVision (Cat no. K178-100). Antibodies against IL-1β (Cat no. ab283818), CD-61 (Cat no. ab17507), GPVI (Cat no. ab289964), GAPDH (Cat no. 8245), and CD62P (Cat no. ab255822) were purchased from Abcam. Antibodies against GFAP (Cat no. 16825-1-AP), CD42b (Cat no. 12860-1-AP) were products of Proteintech. P2Y12 receptor inhibitor, Clopidogrel (Cat no. HY-15283), and FM4-64 were purchased from MCE Chemicals (Shanghai, China). Tirofiban (Cat no. T855553) was a product of Shanghai Maclean Biochemical Technology Co., Ltd. (China). Flow cytometry antibody PE labeled CD62P (Cat no. 148305) or PC5.5 labeled CD61 (Cat no. 104319) were products of BioLegend. FITC Annexin V apoptosis detection kit (Cat no. 556547) was obtained from BD Biosciences. Calcein-AM and all reagents of reverse transcription-polymerase chain reaction (RT-PCR) were obtained from Mei5bio. Besides, fluorescent dye Dil (Cat no. L3482) was acquired from ThermoFisher Scientific.

Male C57BL/6 mice (6−8 weeks, 20−21 g) were acquired from the animal laboratory in Faculty of Health Sciences (FHS), University of Macau and housed at 21 ± 1 °C (room temperature) with humidity of 50 ± 5%, light−dark cycles with 12/12 h, and free access to chow and water. All animal procedures were supported by the Animal Ethics Committee, University of Macau, and the ethics number is UMARE-004-2021. All studies were conducted on the basis of the guidance of National Institutes of Health guide for care and use of Laboratory animals (NIH Publications No. 8023, revised 1978).

Extraction and Preparation of Cryo-Shocked PLT. Platelets from C57BL/6J mice were isolated and analyzed by flow cytometry and western blot (WB) as previously reported.[54] Briefly, platelets were isolated by low velocity centrifugation. To avoid the activation of platelets, antiplatelet aggregation Prostaglandin I_2 (PGI_2, 10 μM, pH 7.4) was administered to acid citrate dextrose (ACD) solution. After isolation, platelets were washed with phosphate-buffered saline (PBS) buffer three times to remove PGI_2. Subsequently, preactivated platelets were obtained after stimulation with 2 U mL^{-1} thrombin and 8 nM $CaCl_2$ for 10 min at 37 °C. Then, cryo-shocked platelets (CsPLT) were prepared by suspending platelets with 2% dimethyl sulfoxide in PBS buffer and immersing in liquid nitrogen for 12 h. Then, the frozen platelets were thawed at 37 °C and centrifuged at 3000 rpm for 2 min. CsPLT was collected after being washed with PBS at least three times.

Viability of Live PLT and Cryo-Shocked PLT. The viability of platelets before and after cryo-shock was determined using Calcein-AM and FM4-64 fluorescent dyes, as was previously reported.[55] Briefly, live platelets and cryo-shocked platelets were incubated with Calcein-AM (2 μM) and FM4-64 (2 μM) for 10 min at 37 °C. Then, after these samples were washed with PBS buffer three times, the fluorescence images and flow cytometry were taken to analyze the dead platelets.

Preparation of Cryo-Shocked PLT Carried ROS-Responsive Liposomes. To acquire CsPLT-CB [7], DSPE-PEG-CB [7] was modified on the surface of CsPLT after incubation for different times (0, 1, 2, 4, 6, 8, or 12 h) at 37 °C, and the undecorated DSPE-PEG-CB [7] was removed by washing with PBS at least three times. Then, the inserted CB [7] on platelet surface was measured by flow cytometry after incubation with Ada-FITC for 5 min. The amantadine (Ada) coupled DSPE−Se−Se-PEG 2000 was synthesized by DSPE−Se−Se-PEG-NHS and Ada-NH_2 via ester−amide reaction and characterized by ^{1}H NMR spectroscopy. Then, an ROS-responsive liposome was achieved with the mole ratio of soybean lecithin, DSPE−Se−Se-PEG-Ada, and cholesterol at 45:5:36. The host−guest system CsPLT-Ada-Se-lipo was prepared by incubation of CsPLT-CB [7] with FITC-labeled Ada-Se-lipo for 0, 1, 2, 5, 15, 30, or 60 min, respectively. CsPLT served as a negative control. Subsequently, flow cytometry was utilized to determine the optimal incubation time. For preparation of ASA and tPA-loaded CPSAT, ASA was added before the formation of lipid membrane, and tPA was dissolved in hydrated PBS solution. Finally, CsPLT-CB [7], CsPLT-Ada-Se-lipo, and CPSAT were characterized by TEM, confocal laser scanning microscopy (CLSM), and western blot analysis.[56]

Measurement for the Quantity of CB [7] on CsPLT-CB [7]. The quantity of CB [7] on the surface of CsPLT-CB [7] was measured indirectly by detection of the combined oxaliplatin. Platinum (Pt) in biological fluids could be decided by inductively coupled mass spectrometry (ICP-MS) as reported.[57] Basically, a series concentration of Pt was prepared to specify the standard curve, and CsPLT-CB[7]-Pt was prepared and diluted to 1:1000 (v/v) with 1% HNO_3.

Quantification of the Content of Liposomes on CPSAT. The concentration of Dil was determined by measuring the optimum absorbance at 549 nm using a UV−vis spectrophotometer.[58] The quantity of Ada-Se-lipo was indirectly measured by quantifying the labeled fluorescent dye Dil. Briefly, the calibration curve of the fluorescent dye was established at 549 nm for standardization. Then, the fluorescently labeled 10 mg/mL Ada-Se-lipo was obtained by an extrusion method. After incubating with 10^7/mL platelets at an equivalent volume for 15 min, CPSAT was obtained after centrifugation for 5 min at 3000 rpm. The contents of fluorescent liposome and CPSAT were calculated by measuring the fluorescence intensity.

Drug Loading and Drug Release of CPSAT. Encapsulation efficiency (EE%) and drug loading capacity (DLC%) in ROS-responsive liposomes were measured as described.[45] The EE% of tPA was quantified by estimating the amidolytic activity, and the EE% of ASA was measured by high-performance liquid chromatography (HPLC) with a reverse-phase C18 column (Agilent Zorbax SB-C18) by using 80:20 (v/v) ratio of a water/acetonitrile mixture containing 0.1% phosphoric acid at 1 mL/min constant flow rate and detection at 220 nm as described previously.[59] EE% and DLC% were measured by the equations

$$\mathrm{EE\%} = \frac{\mathrm{Men}}{\mathrm{Mad}} \times 100$$

$$\mathrm{DLC\%} = \frac{\mathrm{Men}}{\mathrm{Mtotal}} \times 100$$

Men: the quality of encapsulated drug.
Mad: the quality of added drug.
Mtotal: the quality of total ROS-responsive liposomes.

To assess the drug release of ASAT, ROS-responsive liposome was stimulated by 0,10, and 100 mM H_2O_2 for 12 h. After stimulation, the morphology and size distribution of the Ada-Se-lipo were detected by TEM and dynamic light scattering (DLS), and the amount of drug in the supernatant was analyzed by tPA amidolytic activity[45] and HPLC[60] (UV: 235 nm), respectively.

CPSAT Binding to Activated Platelets In Vitro. For flow cytometry, the activated platelets were obtained by stimulation with 8 nM calcium and 2 U/mL thrombin and labeled with CD62P-PE for 15

https://doi.org/10.1021/acsnano.2c11865
ACS Nano 2023, 17, 6519−6533

min. The Ada-Se-lipo, CsPLT-Ada-Se-lipo, or CPSAT were labeled with FITC encapsulated in liposome. To measure the binding to activated platelets, the FITC-labeled Ada-Se-lipo, CsPLT-Ada-Se-lipo, and CPSAT were incubated with PE-labeled activated platelets for 15 min. Subsequently, the unbound Ada-Se-lipo, CsPLT-Ada-Se-lipo, and CPSAT were removed by washing three times and analyzed immediately.

Inhibition Efficacy of CPSAT on Activated Platelets In Vitro. To analyze the inhibition efficacy of CPSAT on activated platelets, the fresh isolated platelets (at concentration of 10^7/mL) were incubated with Ada-Se-lipo, CsPLT-Ada-Se-lipo, and CPSAT (with CsPLT at the same concentration, 10^7/mL). Subsequently, the 8 nM calcium and 2 U/mL thrombin were added to activate platelets for 15 min, followed by being labeled with CD62P-PE. Then, all samples were analyzed by flow cytometry. Besides, the inhibition of CPSAT on inactivation platelets was conducted with the stimulation of 8 nM calcium and 2 U/mL thrombin.

Platelet Aggregation Evaluation. Testing assay of platelet aggregation rate followed as described under the stimulation with adenosine 5′-diphosphate (ADP).[61] Briefly, fresh isolated platelet-rich plasma (PRP, at concentration of 10^7/mL) was obtained from C57BL/6J mice after centrifugation for 15 min. Platelet poor plasma (PPP) was acquired after centrifugation for 25 min at 4000 rpm. One milliliter of PRP was added into a cuvette and incubated with CPSAT (at the concentration of 2 mg/mL CsPLT) followed by the addition of ADP (10 μM). Then the changes of transmittance by detecting the absorbance at 650 nm were recorded every minute for 1 h. Negative control (PRP) was adjusted to 0% without stimulation of ADP, and positive control (PPP) was adjusted to 100%. The aggregation rate (%) was measured by the following equation

$$\text{Aggregation Rate\%} = \frac{\text{ODprp} - \text{ODsample}}{\text{ODprp} - \text{ODppp}} \times 100$$

where ODprp is the absorbance of PRP, ODsample is the absorbance of sample, and ODprp is the absorbance of PPP.

Screening Receptors of CPSAT Binding to Activated Platelets. To figure out the receptors contributed to the binding of CPSAT to activated platelets, activated platelets were labeled with CD62P-PE. The already prepared Ada-Se-lipo, CsPLT-Ada-Se-lipo, and CPSAT were labeled with FITC for 15 min, and inhibitors or antibodies, such as tirofiban (20 μM), anti-CD61 antibody (20 μM), anti-CD62P antibody (20 μM), anti-GPVI (20 μM), anti-CD42b (20 μM), and Clopidogrel (20 μM), were added to inhibit the GPIIb/IIIa, CD61, CD62P, GPVI, CD42b, and P2Y12 receptors in CPSAT, respectively. The FITC-labeled CPSAT was finally incubated with PE-labeled activated platelets for 30 min. Then, the binding of CPSAT to activated platelets was analyzed by flow cytometry.

In Vitro Anti-Inflammation Effect of CPSAT. To verify the therapeutic efficacy, the anti-inflammatory properties of the therapeutic system at the cellular level were investigated. Briefly, RAW264.7 cells were seeded and cultured for 24 h. Lipopolysaccharide (LPS,100 ng/mL) and correspondingly administered agents (Saline, 0.4 mg/mL ASA, 0.6 mg/mL tPA, 0.4 mg/mL ASA+ 0.6 mg/mL tPA, 0.6 mg/mL AST, 1.0 mg/mL ASAT, 0.6 mg/mL CPST, and 1.0 mg/mL CPSAT) were added into the cells for 12 h of incubation. Subsequently, relative expressions of TNF-α and IL-1β in cells were determined via immunofluorescence analysis. The concentrations of relative pro-inflammatory cytokines such as TNF-α, IL-1β, and IL-6 were assayed by an enzyme-linked immunosorbent assay (ELISA). Besides, the mRNA expressions of TNF-α, IL-1β, and IL-6 were evaluated by RT-PCR.

Targeting and Therapeutic Effects of CPSAT in Ferric Chloride-Induced Thrombosis on Mesentery Vessel. The mechanism for the ferric chloride ($FeCl_3$)-induced thrombosis model is attributed to the free radicals caused by the damage of endothelial cells that was first established on the vessels.[62] Damaged vessels trigger the activation, aggregation, and adhesion of platelets or the recruitment of leukocytes, particularly neutrophils.[63] Before establishment of the model, C57BL/6J mice (6−8 weeks old, 20−21 g) were anaesthetized under oxygen with 3% isoflurane for 10 min and maintained with 1% isoflurane by wearing a gas anesthesia mask in a stereotaxic frame. Subsequently, 100 μL of Rhodamine 6 G (Rho 6 G, 0.1%, w/v) was intravenously injected into the mouse before surgery to label platelets. After we carefully cut the peritoneum to expose the mesenteric arteries, one of intestinal arteries was careful spread on the dish, and the fluorescence microscope was taken to visualize the dynamic of labeled platelets. Then, 6% (w/v) $FeCl_3$ was incubated carefully onto the arteriole with forceps for 10 s. Formation of thrombus was observed (at peak excitation 557 nm, peak emission 576 nm) by fluorescence microscopy.

To evaluate the targeting effects on thrombosis in mesenteric artery, FITC-labeled Ada-Se-lipo, CsPLT-Ada-Se-lipo, and CPSAT (doses equivalent to 1.0 mg/kg FITC) were injected in mice. The fluorescence of Rho 6 G was recorded to reflect the thrombus formation, and the FITC was detected after formatting visible thrombus within 1 h. To assess the thrombolysis of CPSAT before and after formation of the thrombus, the Saline, tPA (3 mg/kg), A+T (2 mg/kg ASA+ 3 mg/kg tPA), AST (3 mg/kg), ASAT (2 mg/kg ASA+ 3 mg/kg tPA), CPST (3 mg/kg tPA), and CPSAT (2 mg/kg ASA+ 3 mg/kg tPA) were injected by tail vein. All these fluorescence intensities were analyzed using LASX software (Leica).

Targeting and Therapeutic Effects of CPSAT in Photochemically Induced Ischemic Stroke. A photochemically induced acute stroke mice model was established and evaluated as previously.[45] Targeting efficiency evaluation was achieved after 1.5 h established mice model with Cy5.5-labeled Ada-Se-lipo, CsPLT-CB [7], and CsPLT-Ada-Se-lipo (at dose of 0.5 mg/kg Cy5.5). For therapeutic effects, the Saline, tPA (3 mg/kg), A+T (2 mg/kg ASA+ 3 mg/kg tPA), AST (3 mg/kg), ASAT (2 mg/kg ASA+ 3 mg/kg tPA), CPST (3 mg/kg tPA), and CPSAT (2 mg/kg ASA+ 3 mg/kg tPA) were injected into stroke mice by tail vein. During 7 days of postadministration, the behavioral assessment, infarction volume, and cerebral blood flow were observed by mNSS, Catwalk XT (Noldus), optical coherence tomography (OCT, Thorlabs, TELESTO-II-1325LR) imaging,[64] T2WI nuclear magnetic resonance imaging (MRI, Aspect M3 MRI system), or laser speckle imaging (LSI, RWD, RFSLI ZW/RFLS III) as we had described. At the end of the experiment, mice were sacrificed to measure the infarct volume by TTC staining (2% m/v in PBS), and BBB permeability (Evans blue leakage, 2% m/v in PBS, 4ml/kg) was assessed by an IVIS imaging system (PerkinElmer, IVIS@ Lumina XR, Series III). H&E staining and Nissl staining were taken to examine the pathological abnormal at cellular level. D-dimer levels were measured by ELISA as described.[65] Potential toxicity was measured by analyzing the pathological changes of major organs (spleen, kidney, lung, heart, or liver) and the typical indexes of liver and kidney functions (ALT, AST, TP, CRE, or UREA) as well as four coagulation indicators (aPTT, TT, PT, or FIB).

Assessment of Brain Tissue Immunofluorescence. Mice brains were processed for frozen section at thickness of 20 μm, then immunofluorescence staining was performed by using antibodies. Neuronal survival and cell apoptosis at the infarct site were characterized by Brdu and NeuN. Anti-inflammation effects were measured by the activation of astrocyte, microglial or recruited macrophage polarization, and neutrophil infiltration with GFAP, Iba-1, and Gr-1 antibodies, respectively.

Statistical Analysis. All results were shown as mean ± standard deviation (SD). Statistics were analyzed by GraphPad Prism 9.0, and differences between groups were compared by one-way analysis of variance (ANOVA) with a posthoc test. *$P \leq 0.05$, **$P \leq 0.01$, ***$P \leq 0.001$, and ****$P \leq 0.0001$.

ASSOCIATED CONTENT

Supporting Information

The Supporting Information is available free of charge at https://pubs.acs.org/doi/10.1021/acsnano.2c11865.

Characterizations of native, thrombin-activated, and cryo-shocked activated platelets; comparations of the proteins and targeting efficiency of live platelets and cryo-shocked platelets; synthesis and ^{1}H NMR spectrum of DSPE−Se−

https://doi.org/10.1021/acsnano.2c11865
ACS Nano 2023, 17, 6519−6533

Se-PEG-Ada; stability assessment of bare Ada-Se-lipo and drugs loaded ASAT; stability of CsPLT-CB [7]; targeting efficiency of CsPLT-CB [7] to stroke site; qualification of Ada-Se-lipo on the surface of CsPLT; in vitro binding with activated platelets and inhibition of the platelet activation by CPSAT; receptors analysis of CPSAT contributed to binding with activated platelets; therapeutic efficacy of ASA, CsPLT-CB [7], Ada-Se-lipo, and CsPLT-Ada-Se-lipo in mesenteric thrombosis model and ischemic stroke model; relative D-dimer level in ischemic stroke mice after treatment; relative fluorescence quantification for Brdu, NeuN, GFAP, Iba-1, and Gr-1 in stroke mice brain slices; anti-inflammatory of ASA in ischemic stroke mice brain (PDF)

AUTHOR INFORMATION

Corresponding Authors

Ruibing Wang − *State Key Laboratory of Quality Research in Chinese Medicine, Institute of Chinese Medical Sciences and Department of Pharmaceutical Sciences, Faculty of Health Sciences, University of Macau, Macau, SAR 999078, China;* orcid.org/0000-0001-9489-4241; Email: rwang@um.edu.mo

Yonghua Zhao − *State Key Laboratory of Quality Research in Chinese Medicine, Institute of Chinese Medical Sciences and Department of Pharmaceutical Sciences, Faculty of Health Sciences, University of Macau, Macau, SAR 999078, China;* orcid.org/0000-0001-8714-0476; Email: yonghuazhao@um.edu.mo

Authors

Xingping Quan − *State Key Laboratory of Quality Research in Chinese Medicine, Institute of Chinese Medical Sciences, University of Macau, Macau, SAR 999078, China*

Xiao Liang − *Cancer Center, Faculty of Health Sciences, University of Macau, Macau, SAR 999078, China;* orcid.org/0000-0003-1967-362X

Yuanfu Ding − *State Key Laboratory of Quality Research in Chinese Medicine, Institute of Chinese Medical Sciences, University of Macau, Macau, SAR 999078, China*

Yan Han − *State Key Laboratory of Quality Research in Chinese Medicine, Institute of Chinese Medical Sciences, University of Macau, Macau, SAR 999078, China*

Junyan Li − *State Key Laboratory of Quality Research in Chinese Medicine, Institute of Chinese Medical Sciences, University of Macau, Macau, SAR 999078, China*

Mengchen Yuan − *State Key Laboratory of Quality Research in Chinese Medicine, Institute of Chinese Medical Sciences, University of Macau, Macau, SAR 999078, China*

Yiyang Li − *State Key Laboratory of Quality Research in Chinese Medicine, Institute of Chinese Medical Sciences, University of Macau, Macau, SAR 999078, China*

Zhen Yuan − *Cancer Center, Faculty of Health Sciences, University of Macau, Macau, SAR 999078, China;* orcid.org/0000-0003-3061-6263

Complete contact information is available at: https://pubs.acs.org/10.1021/acsnano.2c11865

Author Contributions

The manuscript was written through contributions of all authors. All authors have given approval to the final version of the manuscript.

Notes

The authors declare no competing financial interest.

ACKNOWLEDGMENTS

This work was supported by the University of Macau (MYRG-CRG2022-00011-ICMS, MYRG-GRG2022-00081-ICMS, and MYRG-GRG2022-00221-ICMS), the National Natural Science Foundation of China (NSFC No. 82074051), the Science and Technology Development Fund, Macau SAR (File Nos. 0065/2021/A2, 0086/2022/A2, and 0045/2021/A1), Shenzhen Science and Technology Innovation Committee (EF023/ICMS-WRB/2022/SZSTIC), and the State Key Laboratory of Quality Research in Chinese Medicine (UM) Internal Research Grant (IRG) 2022 (QRCM-IRG2022-029 and QRCM-IRG2022-024). We are grateful to Prof. Greta SP Mok of University of Macau for her assistance on interpretation of biomedical imaging data. All animal procedures were approved by the Animal Ethics Committee, University of Macau (UMARE-034-2020).

REFERENCES

(1) Gailani, D.; Renné, T. The Intrinsic Pathway of Coagulation: a Target for Treating Thromboembolic Disease? *J. Thromb. Haemostasis* **2007**, *5*, 1106−1112.

(2) Ottinger, L. W. Mesenteric Ischemia. *N. Engl. J. Med.* **1982**, *307*, 535−537.

(3) Wendelboe, A. M.; Raskob, G. E. Global Burden of Thrombosis: Epidemiologic Aspects. *Circ. Res.* **2016**, *118*, 1340−1347.

(4) Mackman, N. Triggers, Targets and Treatments for Thrombosis. *Nature* **2008**, *451*, 914−918.

(5) Wolberg, A. S.; Rosendaal, F. R.; Weitz, J. I.; Jaffer, I. H.; Agnelli, G.; Baglin, T.; Mackman, N. Venous Thrombosis. *Nat. Rev. Dis. Primers* **2015**, *1*, 15006.

(6) Feske, S. K. Ischemic Stroke. *Am. J. Med.* **2021**, *134*, 1457−1464.

(7) Mastoraki, A.; Mastoraki, S.; Tziava, E.; Touloumi, S.; Krinos, N.; Danias, N.; Lazaris, A.; Arkadopoulos, N. Mesenteric Ischemia: Pathogenesis and Challenging Diagnostic and Therapeutic Modalities. *World J. Gastroenterol.* **2016**, *7*, 125−130.

(8) Huang, L.; Zhang, L. Neural Sem Cell Therapies and Hypoxic-ischemic Brain Injury. *Prog. Neurobiol.* **2019**, *173*, 1−17.

(9) Yang, J. L.; Mukda, S.; Chen, S. D. Diverse Roles of Mitochondria in Ischemic Stroke. *Redox Biol.* **2018**, *16*, 263−275.

(10) Mittal, M.; Siddiqui, M. R.; Tran, K.; Reddy, S. P.; Malik, A. B. Reactive Oxygen Species in Inflammation and Tissue Injury. *Antioxid. Redox Signal.* **2014**, *20*, 1126−1167.

(11) Patrono, C.; Baigent, C. Role of Aspirin in Primary Prevention of Cardiovascular Disease. *Nat. Rev. Cardiol.* **2019**, *16*, 675−686.

(12) Lucotti, S.; Cerutti, C.; Soyer, M.; Gil-Bernabé, A. M.; Gomes, A. L.; Allen, P. D.; Smart, S.; Markelc, B.; Watson, K.; Armstrong, P. C.; Mitchell, J. A.; Warner, T. D.; Ridley, A. J.; Muschel, R. J. Aspirin Blocks Formation of Metastatic Intravascular Niches by Inhibiting Platelet-derived COX-1/Thromboxane A2. *J. Clin. Invest.* **2019**, *129*, 1845−1862.

(13) Faour, M.; Piuzzi, N. S.; Brigati, D. P.; Klika, A. K.; Mont, M. A.; Barsoum, W. K.; Higuera, C. A. Low-Dose Aspirin Is Safe and Effective for Venous Thromboembolism Prophylaxis Following Total Knee Arthroplasty. *J. Arthroplasty* **2018**, *33*, S131−S135.

(14) Pulmonary Embolism Prevention (PEP) trial Collaborative Group. Prevention of Pulmonary Embolism and Deep Vein Thrombosis with Low Dose Aspirin: Pulmonary Embolism Prevention (PEP) Trial. *Lancet* **2000**, *355*, 1295−1302.

(15) Russo, N. W.; Petrucci, G.; Rocca, B. Aspirin, Stroke and Drug-Drug Interactions. *Vasc. Pharmacol.* **2016**, *87*, 14−22.

(16) Wan, T.; Zhang, Y.; Yuan, K.; Min, J.; Mou, Y.; Jin, X. Acetylsalicylic Acid Promotes Corneal Epithelium Migration by Regulating Neutrophil Extracellular Traps in Alkali Burn. *Front. Immunol.* **2020**, *11*, 551057.

(17) Mao, L.; Li, P.; Zhu, W.; Cai, W.; Liu, Z.; Wang, Y.; Luo, W.; Stetler, R. A.; Leak, R. K.; Yu, W.; Gao, Y.; Chen, J.; Chen, G.; Hu, X. Regulatory T Cells Ameliorate Tissue Plasminogen Activator-Induced Brain Haemorrhage after Stroke. *Brain* **2017**, *140*, 1914−1931.
(18) Shi, K.; Zou, M.; Jia, D. M.; Shi, S.; Yang, X.; Liu, Q.; Dong, J. F.; Sheth, K. N.; Wang, X.; Shi, F. D. tPA Mobilizes Immune Cells That Exacerbate Hemorrhagic Transformation in Stroke. *Circ. Res.* **2021**, *128*, 62−75.
(19) Kim, J. Y.; Kim, J. K.; Park, J. S.; Byun, Y.; Kim, C. K. The Use of PEGylated Liposomes to Prolong Circulation Lifetimes of Tissue Plasminogen Activator. *Biomaterials* **2009**, *30*, 5751−5756.
(20) Blasi, P.; Giovagnoli, S.; Schoubben, A.; Ricci, M.; Rossi, C. Solid Lipid Nanoparticles for Targeted Brain Drug Delivery. *Adv. Drug Delivery Rev.* **2007**, *59*, 454−477.
(21) Leach, J. K.; Patterson, E.; O'Rear, E. A. Encapsulation of a Plasminogen Activator Speeds Reperfusion, Lessens Infarct and Reduces Blood Loss in a Canine Model of Coronary Artery Thrombosis. *Thromb. Haemostasis* **2004**, *91*, 1213−1218.
(22) Chung, T. W.; Wang, S. S.; Tsai, W. J. Accelerating Thrombolysis with Chitosan-coated Plasminogen Activators Encapsulated in Poly-(lactide-co-glycolide) (PLGA) Nanoparticles. *Biomaterials* **2008**, *29*, 228−237.
(23) Refaat, A.; del Rosal, B.; Palasubramaniam, J.; Pietersz, G.; Wang, X.; Moulton, S. E.; Peter, K. Near-Infrared Light-Responsive Liposomes for Protein Delivery: Towards Bleeding-Free Photothermally-Assisted Thrombolysis. *J. Controlled Release* **2021**, *337*, 212−223.
(24) Yang, B.; Chen, Y.; Shi, J. Reactive Oxygen Species (ROS)-Based Nanomedicine. *Chem. Rev.* **2019**, *119*, 4881−4985.
(25) Wan, M.; Wang, Q.; Wang, R.; Wu, R.; Li, T.; Fang, D.; Huang, Y.; Yu, Y.; Fang, L.; Wang, X.; Zhang, Y.; Miao, Z.; Zhao, B.; Wang, F.; Mao, C.; Jiang, Q.; Xu, X.; Shi, D. Platelet-Derived Porous Nanomotor for Thrombus Therapy. *Sci. Adv.* **2020**, *6*, eaaz9014.
(26) Yang, B.; Chen, Y.; Shi, J. Mesoporous Silica/Organosilica Nanoparticles: Synthesis, Biological Effect and Biomedical Application. *Mater. Sci. Eng. R Rep.* **2019**, *137*, 66−105.
(27) Hofmann-Amtenbrink, M.; Grainger, D. W.; Hofmann, H. Nanoparticles in Medicine: Current Challenges Facing Inorganic Nanoparticle Toxicity Assessments and Standardizations. *Nanomedicine* **2015**, *11*, 1689−1694.
(28) Fang, R. H.; Jiang, Y.; Fang, J. C.; Zhang, L. Cell Membrane-derived Nanomaterials for Biomedical Applications. *Biomaterials* **2017**, *128*, 69−83.
(29) Li, J.; Kataoka, K. Chemo-Physical Strategies to Advance the in Vivo Functionality of Targeted Nanomedicine: The Next Generation. *J. Am. Chem. Soc.* **2021**, *143*, 538−559.
(30) Yin, N.; Zhao, Y.; Liu, C.; Yang, Y.; Wang, Z. H.; Yu, W.; Zhang, K.; Zhang, Z.; Liu, J.; Zhang, Y.; Shi, J. Engineered Nanoerythrocytes Alleviate Central Nervous System Inflammation by Regulating the Polarization of Inflammatory Microglia. *Adv. Mater.* **2022**, *34*, 2201322.
(31) Bashor, C. J.; Hilton, I. B.; Bandukwala, H.; Smith, D. M.; Veiseh, O. Engineering the Next Generation of Cell-Based Therapeutics. *Nat. Rev. Drug Discovery* **2022**, *21*, 655−675.
(32) Koupenova, M.; Kehrel, B. E.; Corkrey, H. A.; Freedman, J. E. Thrombosis and Platelets: an Update. *Eur. Heart J.* **2016**, *38*, 785−791.
(33) Spiess, B. D. Platelet Transfusions: The Science Behind Safety, Risks and Appropriate Applications. *Best Pract. Res., Clin. Anaesthesiol.* **2010**, *24*, 65−83.
(34) Wang, S.; Wang, R.; Meng, N.; Lu, L.; Wang, J.; Zhou, J.; Lu, J.; Xu, Q.; Xie, C.; Zhan, C.; Li, Y.; Yu, Y.; Lu, W.; Liu, M. Engineered Platelets-based Drug Delivery Platform for Targeted Thrombolysis. *Acta Pharm. Sin. B* **2022**, *12*, 2000−2013.
(35) Garraud, O.; Cognasse, F.; Tissot, J. D.; Chavarin, P.; Laperche, S.; Morel, P.; Lefrère, J. J.; Pozzetto, B.; Lozano, M.; Blumberg, N.; Osselaer, J. C. Improving Platelet Transfusion Safety: Biomedical and Technical Considerations. *Blood Transfus.* **2016**, *14*, 109−122.
(36) Ci, T.; Li, H.; Chen, G.; Wang, Z.; Wang, J.; Abdou, P.; Tu, Y.; Dotti, G.; Gu, Z. Cryo-shocked Cancer Cells for Targeted Drug Delivery and Vaccination. *Sci. Adv.* **2020**, *6*, eabc3013.
(37) Wood, B.; Padula, M. P.; Marks, D. C.; Johnson, L. Refrigerated Storage of Platelets Initiates Changes in Platelet Surface Marker Expression and Localization of Intracellular Proteins. *Transfusion* **2016**, *56*, 2548−2559.
(38) Johnson, L.; Reade, M. C.; Hyland, R. A.; Tan, S.; Marks, D. C. In Vitro Comparison of Cryopreserved and Liquid Platelets: Potential Clinical Implications. *Transfusion* **2015**, *55*, 838−847.
(39) Waters, L.; Cameron, M.; Padula, M. P.; Marks, D. C.; Johnson, L. Refrigeration, Cryopreservation and Pathogen Inactivation: an Updated Perspective on Platelet Storage Conditions. *Vox Sang.* **2018**, *113*, 317−328.
(40) Zhao, J.; Xu, B.; Chen, G.; Zhang, Y.; Wang, Q.; Zhao, L.; Zhou, H. Cryopreserved Platelets Augment the Inflammatory Response: Role of Phosphatidylserine- and P-selectin-mediated Platelet Phagocytosis in Macrophages. *Transfusion* **2019**, *59*, 1799−1808.
(41) Ma, N.; Li, Y.; Xu, H.; Wang, Z.; Zhang, X. Dual Redox Responsive Assemblies Formed from Diselenide Block Copolymers. *J. Am. Chem. Soc.* **2010**, *132*, 442−443.
(42) Gao, C.; Cheng, Q.; Li, J.; Chen, J.; Wang, Q.; Wei, J.; Huang, Q.; Lee, S.; Gu, D.; Wang, R. Supramolecular Macrophage-Liposome Marriage for Cell-Hitchhiking Delivery and Immunotherapy of Acute Pneumonia and Melanoma. *Adv. Funct. Mater.* **2021**, *31*, 2102440.
(43) Ding, Y. F.; Huang, Q.; Quan, X.; Cheng, Q.; Li, S.; Zhao, Y.; Mok, G. S. P.; Wang, R. Supramolecularly Functionalized Platelets for Rapid Control of Hemorrhage. *Acta Biomater.* **2022**, *149*, 248−257.
(44) Vunta, H.; Belda, B. J.; Arner, R. J.; Channa Reddy, C.; Vanden Heuvel, J. P.; Sandeep Prabhu, K. Selenium Attenuates Pro-Inflammatory Gene Expression in Macrophages. *Mol. Nutr. Food Res.* **2008**, *52*, 1316−1323.
(45) Quan, X.; Han, Y.; Lu, P.; Ding, Y.; Wang, Q.; Li, Y.; Wei, J.; Huang, Q.; Wang, R.; Zhao, Y. Annexin V-Modified Platelet-Biomimetic Nanomedicine for Targeted Therapy of Acute Ischemic Stroke. *Adv. Healthcare Mater.* **2022**, *11*, 2200416.
(46) Iadecola, C.; Nedergaard, M. Glial Regulation of the Cerebral Microvasculature. *Nat. Neurosci.* **2007**, *10*, 1369−1376.
(47) Attwell, D.; Buchan, A. M.; Charpak, S.; Lauritzen, M.; Macvicar, B. A.; Newman, E. A. Glial and Neuronal Control of Brain Blood Flow. *Nature* **2010**, *468*, 232−243.
(48) Poskanzer, K. E.; Molofsky, A. V. Dynamism of an Astrocyte in Vivo: Perspectives on Identity and Function. *Annu. Rev. Physiol.* **2018**, *80*, 143−157.
(49) Patabendige, A.; Singh, A.; Jenkins, S.; Sen, J.; Chen, R. Astrocyte Activation in Neurovascular Damage and Repair Following Ischaemic Stroke. *Int. J. Mol. Sci.* **2021**, *22*, 4280.
(50) Sofroniew, M. V. Molecular Dissection of Reactive Astrogliosis and Glial Scar Formation. *Trends Neurosci.* **2009**, *32*, 638−647.
(51) Ito, M.; Komai, K.; Mise-Omata, S.; Iizuka-Koga, M.; Noguchi, Y.; Kondo, T.; Sakai, R.; Matsuo, K.; Nakayama, T.; Yoshie, O.; Nakatsukasa, H.; Chikuma, S.; Shichita, T.; Yoshimura, A. Brain Regulatory T Cells Suppress Astrogliosis and Potentiate Neurological Recovery. *Nature* **2019**, *565*, 246−250.
(52) Xiong, X. Y.; Liu, L.; Yang, Q. W. Functions and Mechanisms of Microglia/macrophages in Neuroinflammation and Neurogenesis after Stroke. *Prog. Neurobiol.* **2016**, *142*, 23−44.
(53) Daley, J. M.; Thomay, A. A.; Connolly, M. D.; Reichner, J. S.; Albina, J. E. Use of Ly6G-specific Monoclonal Antibody to Deplete Neutrophils in Mice. *J. Leukocyte Biol.* **2008**, *83*, 64−70.
(54) Aurbach, K.; Spindler, M.; Haining, E. J.; Bender, M.; Pleines, I. Blood Collection, Platelet Isolation and Measurement of Platelet Count and Size in Mice-a Practical Guide. *Platelets* **2019**, *30*, 698−707.
(55) Hartley, P. S.; Savill, J.; Brown, S. B. The Death of Human Platelets During Incubation in Citrated Plasma Involves Shedding of CD42b and Aggregation of Dead Platelets. *Thromb. Haemostasis* **2006**, *95*, 100−106.
(56) Du, H.; Chen, Y.; Hou, X.; Huang, Y.; Wei, X.; Yu, X.; Feng, S.; Wu, Y.; Zhan, M.; Shi, X.; Lin, S.; Lu, L.; Yuan, S.; Sun, L. PLOD2 Regulated by Transcription Factor FOXA1 Promotes Metastasis in NSCLC. *Cell Death Dis.* **2017**, *8*, e3143.

https://doi.org/10.1021/acsnano.2c11865
ACS Nano 2023, 17, 6519−6533

(57) Casetta, B.; Roncadin, M.; Montanari, G.; Furlanut, M. Determination of Platinum in Biological Fluids by ICP-Mass Spectrometry. *At. Spectrosc.* **1991**, *12*, 81−86.
(58) Nor Dyana, Z.; Khairunisak, A. R.; Azlan, A. A. Physical Properties of the Amorphous Silica Encapsulated Fluorescence Dye. *Adv. Mater. Res.* **2013**, *686*, 285−289.
(59) Khodayar, S.; Bardania, H.; Shojaosadati, S. A.; Bagheri, F. Optimization and Characterization of Aspirin Encapsulated Nano-Liposomes. *Iran. J. Pharm. Res.* **2018**, *17*, 11−22.
(60) Sultana, N.; Arayne, M. S.; Ali, K. A.; Nawaz, M. Simultaneous Determination of Clopidogrel and Aspirin by RP-HPLC from Bulk Material and Dosage Formulations Using Multivariate Calibration Technique. *J. Chromatogr. Sci.* **2011**, *49*, 165−169.
(61) Kim, C. J.; Kim, J.; Sabaté Del Río, J.; Ki, D. Y.; Kim, J.; Cho, Y. K. Fully Automated Light Transmission Aggregometry on a Disc for Platelet Function Tests. *Lab Chip* **2021**, *21*, 4707−4715.
(62) Bonnard, T.; Hagemeyer, C. E. Ferric Chloride-Induced Thrombosis Mouse Model on Carotid Artery and Mesentery Vessel. *J. Visualized Exp.* **2015**, *100*, e52838.
(63) Versteeg, H. H.; Heemskerk, J. W. M.; Levi, M.; Reitsma, P. H. New Fundamentals in Hemostasis. *Physiol. Rev.* **2013**, *93*, 327−358.
(64) Lee, J.; Gursoy-Ozdemir, Y.; Fu, B.; Boas, D. A.; Dalkara, T. Optical Coherence Tomography Imaging of Capillary Reperfusion after Ischemic Stroke. *Appl. Opt.* **2016**, *55*, 9526−9531.
(65) Bailey, A. L.; Kang, L. I.; de Assis Barros D'Elia Zanella, L. G. F.; Silveira, C. G. T.; Ho, Y. L.; Foquet, L.; Bial, G.; McCune, B. T.; Duarte-Neto, A. N.; Thomas, A.; Raué, H. P.; Byrnes, K.; Kallas, E. G.; Slifka, M. K.; Diamond, M. S. Consumptive Coagulopathy of Severe Yellow Fever Occurs Independently of Hepatocellular Tropism and Massive Hepatic Injury. *Proc. Natl. Acad. Sci. U. S. A.* **2020**, *117*, 32648−32656.

https://doi.org/10.1021/acsnano.2c11865
ACS Nano 2023, 17, 6519−6533